doi: 10.32131/jes.8.13

Journal of the Earth Simulator, Volume 8, November 2007, 13–25

Regional Climate Projection Experiments on the Baiu Frontal Activity around the Japan Islands Using a Non-Hydrostatic Cloud-System-Resolving Model

Yasutaka Wakazuki[1]*, Sachie Kanada[1], Chiashi Muroi[2], Akihiro Hashimoto[3], Teruyuki Kato[3], Masaomi Nakamura[3], Akira Noda[3], Masanori Yoshizaki[4], and Kazuaki Yasunaga[4]

[1] *Advanced Earth Science and Technology Organization, Tokyo, Japan*
[2] *Japan Meteorological Agency, Tokyo, Japan*
[3] *Meteorological Research Institute, Tsukuba, Japan*
[4] *Institute of Observational Research for Global Change, Japan Agency for Marine-Earth Science and Technology, Yokosuka, Japan*

(Received January 29, 2007; Revised manuscript accepted May 8, 2007)

Abstract Regional climate experiments focusing on the Baiu frontal precipitation were performed on the Earth Simulator using a non-hydrostatic cloud-system-resolving atmospheric model (NHM) with a horizontal resolution of 5 km (5km-NHM) and 1 km (1km-NHM). The outputs of an atmospheric general circulation model (AGCM) with a horizontal resolution of about 20 km were used as the boundary of 5km-NHM. The time-slice method in both the present and future climates was applied for the experiments of the AGCM and NHM. In the present climate experiments, it was evaluated that the precipitation distribution and precipitation frequency spectrum (PFS; frequency with intensities) of the 5km-NHM were well reproduced in comparison with those observed. Here, the AGCM in the present climate well reproduced the large-scale characteristics of the Baiu frontal precipitation. The Intergovernmental Panel on Climate Change (IPCC) A1B CO_2 emission scenario was used to project changes in the precipitation property around the Baiu front due to global warming in the future climate around the end of the 21st Century. The 5km-NHM projects not only an increase in precipitation around Western Japan associated with the elongation of the Baiu front due to global warming but also an intensification of precipitation associated with the enhancement of the convectively unstable stratification. The 1km-NHM experiment demonstrates the effects of the high resolution and shows further quality improvements of the PFS and higher reproducibility of extreme precipitation events associated with the organizations of convective systems than the 5km-NHM experiment.

Keywords: regional climate, non-hydrostatic model, Baiu front, global warming

1. Introduction

Climate changes due to global warming are receiving much attention from the viewpoints of economic activity and the global environment (IPCC, 2001 [1]). Among them, the change in the frequency of intense precipitation is an urgent and important problem. In Japan, intense precipitation is mainly brought by tropical cyclones and the Baiu frontal activity and sometimes results in serious disasters, such as floods. In this study, we focus on the Baiu frontal precipitation. The Baiu is the rainy season in East Asia that is formed by the monsoon circulation in early summer. The Baiu fronts are seen as wide and quasi-stationary zones of precipitation and clouds extending in an east-west direction from China to the Japan Islands. The Baiu front has complicated multi-scale structures in association with precipitation systems (Ninomiya et al. 1992 [2]), and the precipitation processes play an important role in the Baiu frontal activity. The projections of climate changes in precipitation along the Baiu front in the future climate is one of the important social and scientific concerns in Japan.

In general, to project climate changes due to global

* ***Corresponding author***: *Yasutaka Wakazuki, Frontier Research Center for Global Change, Japan Agency for Marine-Earth Science and Technology, 3173-25, Showa-machi, Kanazawa, Yokohama, 236-0001, Japan. E-mail: ywakazki@goo.jp*

warming, atmosphere-ocean coupled general circulation models (CGCM) with well-tuned up physical schemes are used in many studies. The models are integrated with some CO_2 emission scenarios. Kimoto et al. (2005) [3] reported a current result of their climate experiments with an atmosphere-ocean CGCM named the Model for Interdisciplinary Research on Climate (MIROC) calculated on the Earth Simulator (ES), one of the best performance experiments among those recently reported. However, the horizontal resolution on the atmosphere of the experiment was about 110 km. This model can well resolve large-scale atmospheric circulations, but it cannot express the structures of disturbances, such as tropical cyclones and Baiu frontal disturbances.

Another approach to examine the changes in precipitation was performed by Mizuta et al. (2006) [4] and Kusunoki et al. (2006) [5]. Their research group developed a high-resolution atmospheric general circulation model (AGCM) with a horizontal resolution of about 20 km (20km-GCM) on the ES. The 20km-GCM can resolve large-scale disturbances, such as tropical cyclones. Using the time-slice method, the sea surface temperature (SST) was fixed with the exception of seasonal variations, and the cost of required calculations was reduced. Here, the increase of SST in the future climate should be obtained from another result of atmosphere-ocean CGCM with lower resolution. In this manner, for example, the changes in global frequency and property of tropical cyclones could be examined (Yoshimura et al. 2006 [6]; Oouchi et al. 2006 [7]). Their impressive results projected that the number of tropical cyclones would decrease over the Western Pacific Ocean and that the number of intense cyclones would increase in the future climate. The changes in the Baiu frontal activities, as well as that of the cyclones, were also examined (Kusunoki et al. 2006 [5]). The Baiu frontal precipitation was also well simulated by the 20km-GCM, and the results of their analyses are referenced in later sections. However, the horizontal resolution of about 20 km is too large to resolve each of the mesoscale precipitation systems and cumulonimbus clouds, which often cause heavy precipitation events.

One-way downscale nesting experiments of AGCMs are often performed using atmospheric regional climate models (RCMs). RCM experiments have often been used to focus on fine structures in atmospheric fields within the defined domain (e.g., Wang et al. 2004 [8]; Kurihara et al. 2005 [9]; Sasaki et al. 2005 [10]). In the RCM calculation, while high-resolution results are calculated, the domain is limited to a regional scale. The resources of the experiments are due to the computer performances.

In this study, a non-hydrostatic and cloud-system-resolving regional atmospheric model with a horizontal resolution of 5 and 1 km is newly used as the RCM on the ES. In their horizontal grid size, the model should be described as a cloud-system-resolving model rather than a cloud-resolving model. The model can explicitly express convective precipitation phenomena. The success of the experiments is due to the high performance of the ES. By using a non-hydrostatic model, the reproducibility of convective precipitation phenomena is significantly improved. One of the main focuses in this study is the frequency of heavy precipitation in the Baiu season (mainly in June and July) around Japan. In addition, changes in the Baiu frontal precipitation in the future are projected. Several results of this project have already been published as papers (Yoshizaki et al. 2005 [11]; Yasunaga et al. 2005 [12]; Yasunaga et al. 2006 [13]; Wakazuki et al. 2005 [14]; Kanada et al. 2005 [15]; Hashimoto et al. 2005 [16]). In this paper, we introduce some points of their studies and current results of the experimental analyses. In Section 2, the numerical model and experimental design are described. In Section 3, the reproducibility of the present climate state simulated by the non-hydrostatic model with a horizontal resolution of 5 km is examined. In Section 4, projections of regional climate changes in the precipitation associated with the Baiu frontal activity due to the global warming are introduced. In Section 5, an advantage of application of horizontal resolution of 1 km is discussed. Finally, the summary is presented in Section 6.

2. Numerical model and experimental design

To examine the climate changes of the Baiu frontal activities due to global warming, three steps of experiments including two steps of regional climate experiments were conducted. First, global experiments with a time-slice method were performed using an AGCM with a horizontal resolution of 20 km (Mizuta et al. 2006 [4]; Kusunoki et al. 2006 [5]; 20km-GCM). The 20km-GCM assumes a hydrostatic state, and the precipitation is produced by large-scale condensation and sub-grid scale convective parameterization schemes. The 20km-GCM experiments on the ES have the highest resolution among AGCM experiments for climate changes. In the present climate experiment, the observed climatological SST averaged from 1982 to 1993 with a seasonal variation is used as the bottom boundaries of 20km-GCM. Kusunoki et al. (2006) [5] verified that the 20km-GCM could reproduce the Baiu frontal rainband extending from East China to the Japan Islands. In the experiment for future climate (around 2080–2099), on the other hand, the difference in the SST from the present climate is added to the observed climatological SST. The difference was estimated by the

projection using an atmosphere-ocean CGCM (MRI-CGCM-2.3; Yukimoto et al. 2006 [17]), which was developed at the Meteorological Research Institute (MRI) of the Japan Meteorological Agency (JMA), under the A1B CO_2 emission scenario.

Second, regional climate experiments, which are one-way downscale nesting experiments, were performed by a non-hydrostatic cloud-system-resolving model with a horizontal resolution of 5 km in the present and future climates. The lateral boundaries of the regional experiments were made from the outputs of the 20km-GCM experiments. The domain of the regional experiments was 4000 × 3000 km (800 × 600 grids) over East Asia, as shown in Fig. 1. Integrations up to 40 days were performed twice (from 21 May to 29 June and from 20 June to 29 July) every year for 10 years in both the present and future climates.

The regional climate model used in the experiments is the JMA Non-Hydrostatic Model (NHM; Saito et al. 2006 [18]). The NHM was developed for operational numerical weather prediction by the JMA. The configuration of operational prediction of the NHM was introduced by Saito et al. (2006) as that of a 10-km resolution mesoscale model. The NHM used in our climate experiments is optimized for the ES, which is a super computer with vector processors, from the original NHM which was developed for scalar computers. Here, the NHM experiment with a horizontal resolution of 5 km (5km-NHM) requires a computer cost of about 260 node-hours for a 5-day integration on the ES. For the cloud and precipitation processes of the NHM, microphysical processes with five categories of liquid and solid water substances, i.e., cloud water, rain, cloud ice, snow, and graupel, are explicitly calculated with the bulk parameterization (Ikawa and Saito 1991 [19]). A two-moment cloud physical scheme, which predicts the mixing ratio and number concentration, is also applied to hydrometeor categories (Hashimoto et al. 2005 [16]) in our climate experiments. We do not use any cumulus parameterization schemes, although the horizontal grid size is slightly large for resolving each cumulonimbus. The left panels of Fig. 2 show the three-dimensional distributions of hydrometeors in association with a precipitation system simulated over the Kyushu District located in the westernmost part of the Japan Islands, as an example. A large amount of precipitation water is concentrated with a band shape in the lower atmosphere, and cloud water and cloud ice spread widely in the upper-level atmosphere. Thus, the NHM can explicitly express the three-dimensional structure and behavior of hydrometeors associated with precipitation systems.

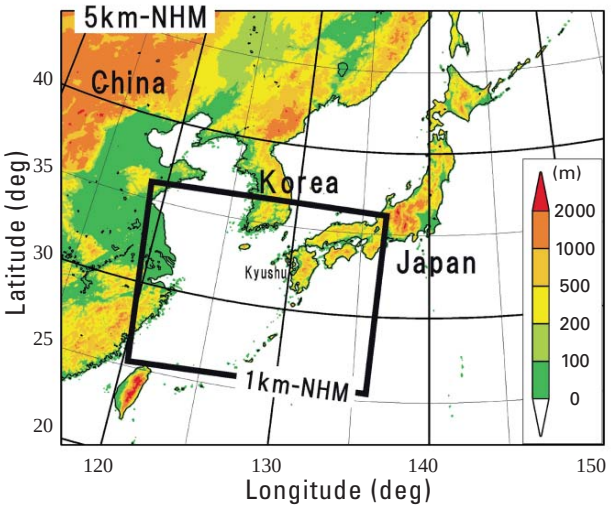

Fig. 1 Domains of numerical experiments of the NHM. The whole-domain and inner-box regions are used for the 5km- and 1km-NHM experiments, respectively. The color is the height of the model topography.

The configuration of our climate experiments with the NHM includes some schemes newly applied for long-term climatological integrations, which are different from those for the operational run. The differences of schemes and configurations of the NHM are summarized in Table 1. One of them is the spectral boundary coupling (SBC) method (Yasunaga et al. 2005 [12]). For long-term integrations of regional models, an adjustment of inconsistencies between the external and internal model states is necessary. For example, differences in the propagations of larger-scale disturbances and those in radiative-convective equilibrium states often cause unnatural and unrealistic precipitation. In the SBC method, the large-scale wave components of internal model values are replaced by those of external model values with an interval. In the experiments, the interval and minimum horizontal scale are configured to be 20 minutes and about 500 km, respectively. The variables replaced by the SBC are U, V, and θ above a height of 5 km in a z*-plane.

Third, NHM experiments with a horizontal resolution of 1 km (1km-NHM), which are also one-way downscale nesting experiments, were performed with the lateral boundaries of 5km-NHM results. The domain of experiment is also shown in Fig. 1. The number of horizontal grids was 1600 × 1200. Integrations up to 18 days were calculated from 30 June to 17 July, in which the Baiu frontal precipitation was significantly present. The calculation had a large computational cost (about 1,425 node-hours for a 3-day integration on the ES). A 1-year experiment was performed for each of the present and future climates. Figure 2 shows the differences in the distribution of hydrometeors associated with the precipitation

Table 1 Schemes and configurations of the NHM in our climate experiments in comparison with those in Saito et al. (2006) [18]. Prognostic variables include x-, y-, and vertical-direction momentums (U, V, W), pressure perturbation (P), potential temperature (θ), and turbulent kinetic energy (E_{TK}) as dynamic parameters. Variables for the moist processes are the mixing ratio of cloud water (qc), cloud ice (qci), rain water (qr), graupel (qg), and snow (qs). In addition, their number concentrations (Nc, Nci, Nr, Ng, Ns) are used.

Schemes	**Routine**; Saito et al. (2006) [18]	**Our Climate Experiments**
Dynamics	Non-hydrostatic	
Basic equations	Full compressible system	
Boundary condition	Rayleigh damping is used for lateral and upper boundaries	
Horizontal discretization	Arakawa C	
Vertical coordinate	Terrain following z^* coordinate	
Schemes of dynamics and physical processes		
Prognostic Variable	$U, V, W, P, \theta, q_v, q_c, q_i, q_r, q_s, q_g$	$U, V, W, P, \theta, E_{TK}, q_v, q_c, q_i, q_r, q_s, q_g, N_c, N_i, N_r, N_s, N_g$
Treatment of sound waves	Horizontally explicit and vertically implicit (HE-VI)	
Advection	Flux form fourth-order with advection correction and time splitting	Flux form second-order with advection correction, No time splitting
Turbulent closure	Diagnostic TKE scheme	Prognostic TKE scheme (Deardorff 1980 [20]), Level 2.5
Convective parameterization	Modified Kain-Fritsch scheme Original: Kain (2004) [21]	None
Moist physics	Three-ice bulk microphysics; Ikawa and Saito (1990) [19]	Three-ice two-moment microphysics; Hashimoto et al. (2005) [16]
Gravity waves	Time splitting	No time splitting
Boundary layer turbulence	Sun and Chang (1986) [22] with anisotropy mixing length	Anisotropy mixing length
Secondary inner forcing	None	Spectral Boundary Coupling (SBC); Yasunaga et al. (2005) [12]
Radiation	Cloud amount is determined by relative humidity.	
Ground temperature	4 layer heat conduction model (bottom layer is climatological constant)	
Land surface flux	Monin-Obukhov similarity law with a bulk coefficient of Louis et al. (1982) [23], Stomatal resistance	
Sea surface flux	Bulk coefficient: Kondo (1975) [24]	Bulk coefficient: Louis et al. (1982) [23], Roughness: Beljaars et al. (1995) [25]
Experiment Design		
Mapping	Lambert conformal projection	
Vertical Grid	40 layers dz is stretched from 40 to 1180 m	48 layers dz is stretched from 40 to 960 m
Horizontal grid size	361×289 (10km)	800×600 (5km)
Horizontal grid size (fine mesh experiment)		1600×1200 (1km)

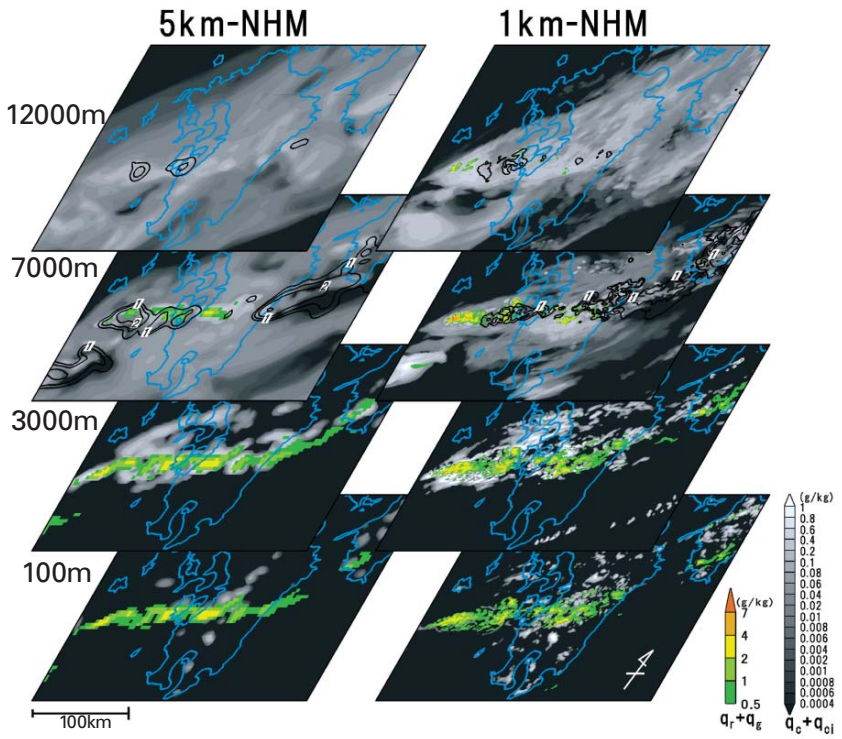

Fig. 2 Three-dimensional distributions of hydrometeors associated with a precipitation system simulated around the Kyushu District located to the westernmost part of the Japan Islands as an example. Colors show the summations of qr and qg. White-black regions show the summations of qc and qci. Solid contours are qs. Left and Right panels are results of 5km- and 1km-NHM experiments, respectively. These maps are sliced at 100, 3,000, 7,000 and 12,000 m levels with a z*-plane.

system between 5km-NHM and 1km-NHM. Fine cellular features of rain water associated with cumulonimbus clouds are found in the 1km-NHM results, although they are not present in the 5km-NHM results. The horizontal size of the cumulonimbus clouds is about 10 km in general. It is considered that the NHM with a horizontal grid size of about 1 km is sufficient to resolve each cumulonimbus. In this calculation, the SBC method is not applied because of the narrow domain.

3. Reproducibility of the present climate state

Radar-raingauge analyzed precipitation (R-A) is used as one of the observed precipitation data for verifications of model outputs. The R-A is precipitation distribution data that is estimated using a meteorological radar network modified by the Automated Meteorological Data Acquisition System (AMeDAS) raingauge data. However, the accumulated precipitation amounts of the R-A are overestimated in comparison with those of AMeDAS even near the AMeDAS point. Figure 3 shows a ratio of the precipitation estimated by the R-A from that estimated by the AMeDAS raingage data averaged with variable grid sizes. The overestimation rate is estimated in this paper to be about 14 %, which is the ratio at the averaging grid size (spatial representativeness) of zero. Here, non-data grids of the R-A (non-observations or errors) are assumed to be non-precipitation ones. This correction method, newly applied in this paper, is simple. The corrected R-A is used for the verifications of the experiment results.

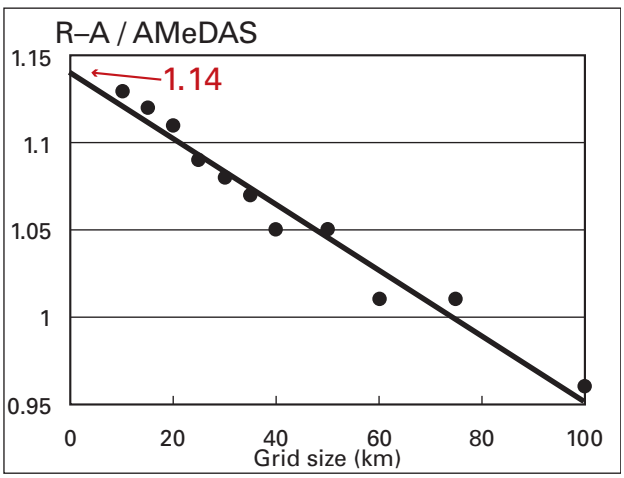

Fig. 3 Ratio of the mean precipitation amount estimated by the R-A to that estimated by AMeDAS raingage data averaged with variable grid sizes.

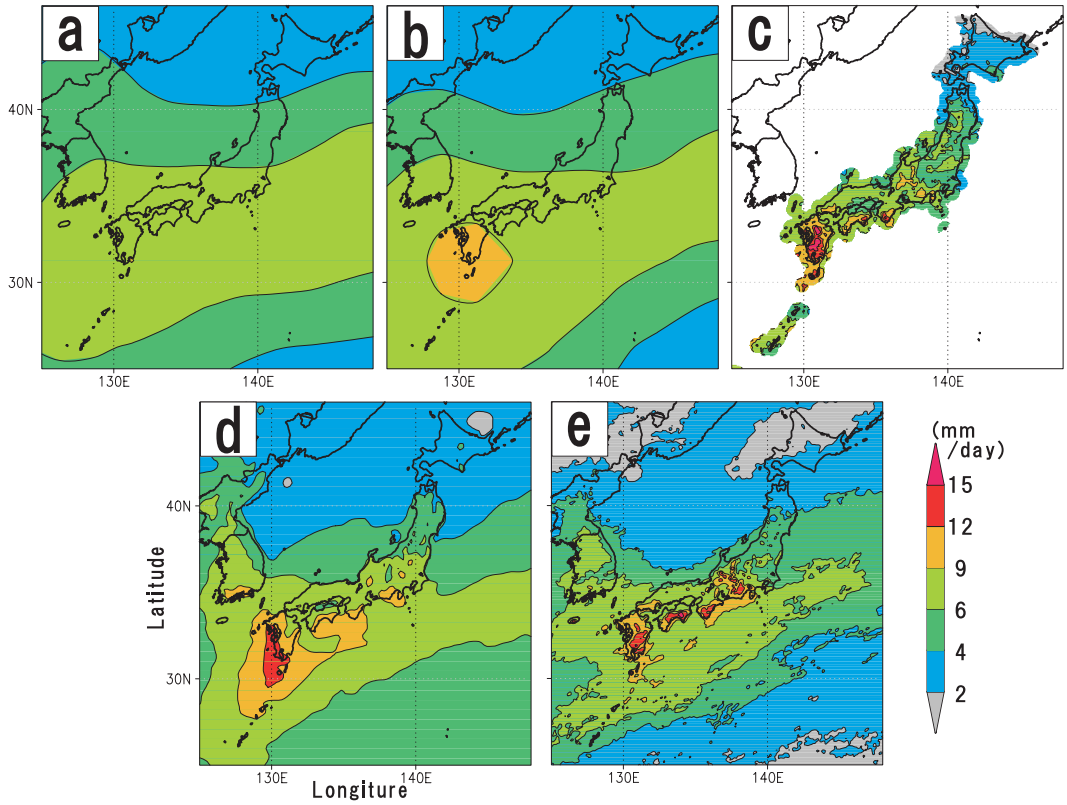

Fig. 4 Observed and simulated precipitation amounts averaged from 22 May to 20 July. (a) Pentad GPCP precipitation averaged from 1982 to 1993. (b) Same as (a) but averaged from 1995 to 2004. (c) Modified R-A precipitation around Japanese main islands averaged from 1995 to 2004. Reproduced precipitations averaged for 10 years in the present climate, which are simulated by (d) 20km-GCM and (e) 5km-NHM.

The results of statistical analysis of 5km-NHM in the present climate are expected to have a quality almost equal to those observed. Figure 4 shows the distributions of precipitation amounts of the corrected R-A, Global Precipitation Climatology Project (GPCP), 20km-GCM, and 5km-NHM within the period from 22 May to 20 July in the present climate. The present climate simulated with the time-slice method is based on the period from 1982 to 1993. On the other hand, the R-A data was created only after 1995. Figures 4a and 4b show that the difference of precipitation distributions in the Baiu season within the period from 1982 to 1993 and that from 1995 to 2004 is not large, except for a slight increase around the Kyushu District. The 20km-GCM (Fig. 4d) roughly reproduces the Baiu frontal precipitation distribution. The 5km-NHM (Fig. 4e) can also reproduce the Baiu frontal precipitation with finer structures. In particular, peaks are found over the Kyushu District and Western Japan along the shoreline of the Pacific Ocean. This characteristic is consistent with that of the R-A precipitation (Fig. 4c). In this area, a large amount of precipitation is brought by the moisture flux along the Baiu front and the anti-cyclonic circulation of the quasi-stationary Pacific high. The moist flow generates convections around the mountain areas over Western Japan. The large-scale characteristics of thermodynamic fields in 5km-NHM should be almost the same as those of 20km-GCM. However the precipitation property of 5km-NHM is largely different from that of 20km-GCM. Here, the precipitation distribution of 5km-NHM seems to express finer structures associated with not only the finer topography but also the explicit precipitation processes of the model because the 5km-NHM can often reproduce precipitation systems with heavy rainfall.

The precipitation property in 5km-NHM around Japan is verified by dividing the area into five sub-regions, as shown in Fig. 5. The precipitation amount in each sub-region in Fig. 6 shows that 5km-NHM well reproduces the observed precipitation amount within each sub-region. A figure similar to Fig. 6 is also shown in Yoshizaki et al. (2005) [11]. They reported problems in which the precipitation amount of 5km-NHM was underestimated. However, the problems are roughly resolved with a correction of the accumulated R-A precipitation

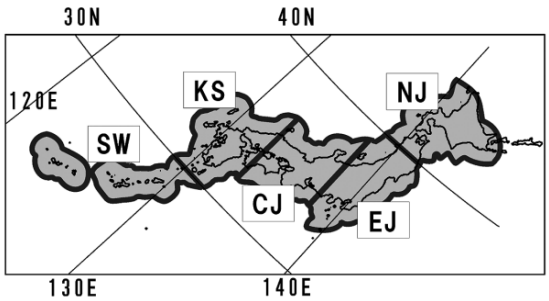

Fig. 5 Distribution of five sub-regions divided from the Japanese area limited to the ranges within 100 km from the AMeDAS points and below 2000 m height of the lowest radar beam centers. This division is also used in Yoshizaki et al. (2005). The sub-regions of SW, KS, CJ, EJ, and NJ mean Southwestern Japan, Kyushu District, Central Japan, Eastern Japan, and Northern Japan, respectively.

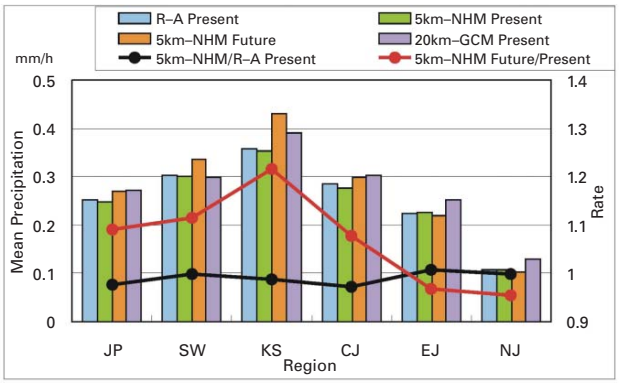

Fig. 6 Precipitation amounts over the divided regions (Fig. 5) averaged from 22 May to 20 July. The blue bars are the observed (corrected R-A) precipitation amounts. The green and purple bars are the precipitation in the present climate reproduced by 5km-NHM and 20km-GCM, respectively. The orange bars are the precipitation in the future climate projected by 5km-NHM. The black line shows the reproducibility of 5km-NHM (5km-NHM (Present climate) / R-A). The red line shows the rate of increase due to the global warming projected by 5km-NHM (Future climate / Present climate). The JP means a total sum region of the five sub-regions.

and a fine-tuning of the NHM. The precipitation amount and the intense precipitation frequency were underestimated as a result of mistakes in the calculation of the NHM that were found after the publication of the study by Yoshizaki et al. (2005) [11]. The precipitation amount of the NHM noted in Fig. 6 is corrected to remove the influence of the mistakes.

Figure 7 shows the precipitation frequency spectrum (PFS) with intensities (mm h^{-1}). The PFS of the 20km-GCM experiments is inconsistent with that of R-A; precipitation in intensities below 3 mm h^{-1} is heavily overes-

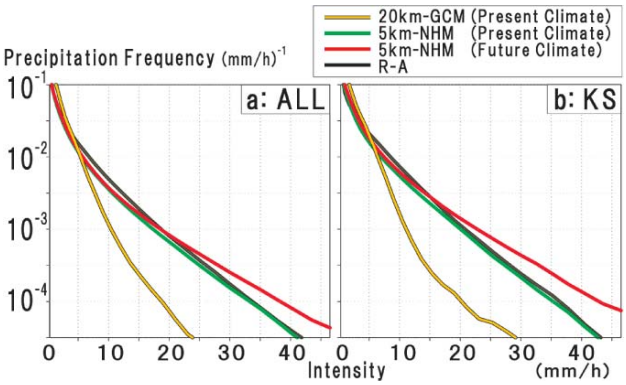

Fig. 7 Precipitation frequencies for variable intensities with a grid size of 20 km. Each integrated area of the curve is equal to 1. They are estimated with a period from 22 May to 20 July for 10 yeas of data. The black, yellow, green, and red lines are R-A, 20km-GCM (Present climate), 5km-NHM (Present climate), and 5km-NHM (Future climate) experiment results, respectively. (a) Left and (b) right panels are results over all regions and the KS region, respectively, in Fig. 5.

timated, while that in intensities above 5 mm h^{-1} is significantly underestimated. Figure 8 shows PFS defined in Fig. 7 for the intensities of 1, 4, and 30 mm h^{-1} with a grid size of 20 km in each sub-region (Fig. 5). Weak and heavy precipitation frequencies, such as 1 and 30 mm h^{-1} of 20km-GCM, are obviously too large and small in all sub-regions, respectively. On the other hand, the PFS of 5km-NHM in Figs. 7 and 8 almost correspond to those of R-A. This shows that the NHM can simulate the realistic precipitation property. However, the reproducibility is not perfect. The PFS of 5km-NHM is slightly underestimated in intensities below 20 mm h^{-1} in comparison with the R-A (Fig. 7). This problem is considered to be mainly caused by a large grid size in the 5km-NHM experiment for precipitation phenomena. Grid scale updrafts simulated by 5km-NHM are considered to be too strong compared with real convections, while the frequency of weak and moderate precipitation decreases. The targeted moisture diffusion (TMD; Saito et al. 2006 [18]) scheme was implemented to suppress excessive updrafts caused by diabatic heating by condensation. In the scheme, water vapor within strong updrafts is diffused. However, the TMD was not sufficient for the PFS to be quite realistic. In Saito et al. (2006) [18], this problem is also noted. They used convective parameterization (modified Kain-Fritsch scheme) as well as an explicit cloud physical scheme in the NHM experiment with a horizontal grid size of 10 km. The combination of those schemes is needed to obtain more realistic simulations with 5km-NHM in future studies.

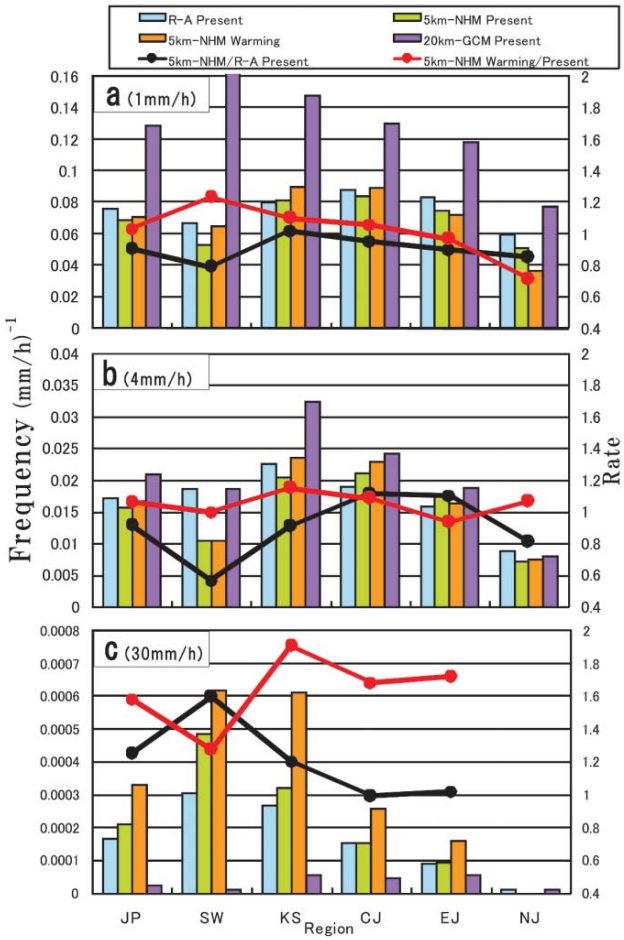

Fig. 8 Precipitation frequencies defined in Fig. 7 over the divided regions (Fig. 5). The intensities are (a) 1mm h^{-1}, (b) 4mm h^{-1}, and (c) 30mm h^{-1} with a grid size of about 20km. The blue bars are the observed (R-A) precipitation frequencies. The green and purple bars are those in the present climate reproduced by 5km-NHM and 20km-GCM, respectively. The orange bars are those in the future climate projected by 5km-NHM. The black line shows the reproducibility of 5km-NHM (5km-NHM (Present climate) / R-A). The red line shows the increase rate due to global warming estimated by 5km-NHM (Future climate / Present climate).

4. Regional climate changes in the Baiu frontal activity

Kusunoki et al. (2005) [5], Yoshizaki et al. (2005) [11], Yasunaga et al. (2006) [13], and Wakazuki et al. (2005) [14] reported that the Baiu season is prolonged and total precipitation amounts along the Baiu front increase in the future climate. Figure 9 shows time-latitude cross sections of surface precipitation amounts averaged within a longitudinal range from 130 to 140 E and for 10 years in the present and future climates simulated by 20km-GCM. In the present climate, the precipitation zone associated with the Baiu front propagates to the north from June to July and becomes unclear in approximately mid-July. On the other hand, in the future climate, the Baiu front is stationary in the latitudinal zone from 30 to 35 N until late July. Consequently, the precipitation amount over Western Japan increases, while that over Northern Japan and the Korean Peninsula decreases in the Baiu season. Changes in precipitation over the sub-regions projected by 5km-NHM are shown in Fig. 6. The precipitation amount in Japan is projected to increase, and the rate of increase is estimated to be about 10% from 22 May to 20 July. In particular, the precipitation amount in the KS region reaches approximately 20%. On the other hand, precipitation in the EJ and NJ regions decreases by about 5%. Kusunoki et al. (2006) [5] discussed the elongation of the Baiu season due to global warming. The future precipitation change is mainly attributable to the changes in the horizontal transport of water vapor flux and its convergence associated with the intensification of a subtropical high. This can be interpreted as an atmospheric response to the El Niño condition of the ocean. Here, MRI-CGCM-2.3 (Yukimoto et al. 2006 [17]) projected the SST change in the future climate similar to the SST anomaly in the El Niño condition (not shown).

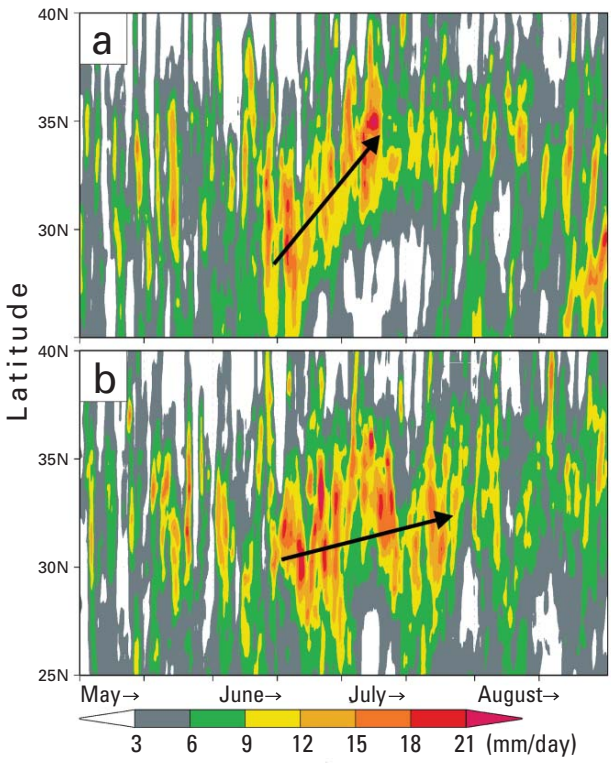

Fig. 9 Time-latitude cross sections of the surface precipitation amount averaged within a longitudinal range of 130–140E and for 10 years of data in the (a) present and (b) future climates. They are projected by 20km-GCM. Inter-diurnal variations are removed. Arrows show schematic feature of propagations of the Baiu frontal precipitation.

Another change in the precipitation property around the Baiu front is the intensification of precipitation due to convectively unstable stratification. Figure 8 shows the rate of increase of the precipitation frequency (red lines). The rates of increase are larger with more intense precipitation. For example, the rate of increase is about 1.9 with an intensity of 30 mm h^{-1} in the KS region. The rate with intensities of 1 and 4 mm h^{-1} is from 0.9 to 1.2. The intensification of precipitation was also reported by Wakazuki et al. (2005) [14]. They noted that the intensification of precipitation was brought by the enhancement of the convectively unstable stratification in the lower atmosphere. This is due to a significant increase of water vapor in the lower atmosphere caused by the temperature increase.

The intensification of precipitation suggests an increase in the diabatic effect associated with disturbances along the Baiu front. Wakazuki et al. (2005) [14] examined the vertical axis of depressions accompanied by strong precipitation along the Baiu front. The increase in the number of eastward tilting depressions was significantly larger than that of westward tilting depressions (not shown). Previous studies have shown that eastward tilting depressions are generated in association with large diabatic effects (*e.g.*, Tokioka, 1973 [26]; Yanase and Niino, 2004 [27]; Tagami, 2005 [28]). This type of depression is frequently observed along the Baiu front. Therefore, the diabatic effect could become larger in the future.

5. Impact of the 1km-NHM experiment

Another grid size in which each cellular deep convective cloud, such as a cumulonimbus, could be resolved is also used in the NHM experiments. A grid size of 1 km was used to produce the desired degree of restriction. The more realistic calculation with a grid size of 1 km results in a better reproduction of PFS. Figure 10 shows the PFS of 1km-NHM experiments compared with that of 5km-NHM. The frequencies of moderate precipitation and heavy precipitation with intensities from 3 to 18 mm h^{-1}

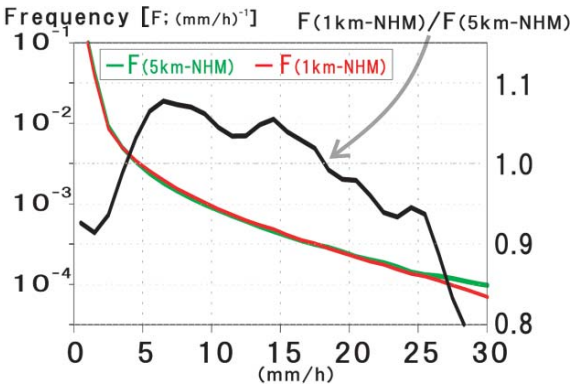

Fig. 10 Precipitation frequencies defined in Fig. 7 of 5km- (green line) and 1km-NHM (red line). These are calculated by two 15-day data sets of the present and future climates with an area of 122–135E, 27–35N. The black line indicates a ratio of PFS of 1km-NHM to that of 5km-NHM.

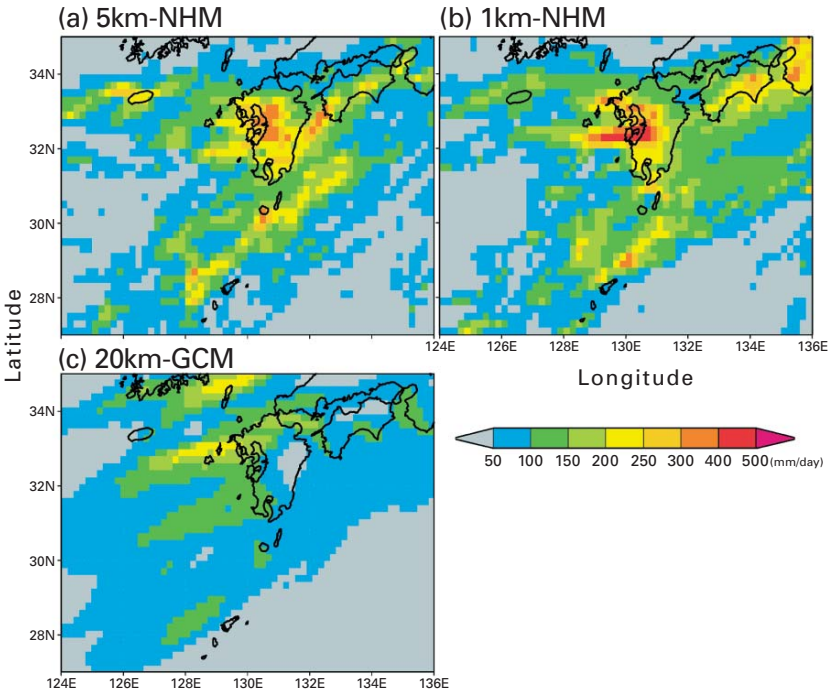

Fig. 11 Distributions of the top values of 24-hour-accumulated precipitation amounts (24h-Top) for (a) 5km-NHM, (b) 1km-NHM, and (c) 20km-GCM. These are selected from a 15-day data set as an example.

and stronger than 18 mm h^{-1} increase and decrease, respectively. The differences in the precipitation property between 5km- and 1km-NHM suggest that the inconsistency between the PFS of 5km-NHM and R-A shown in Fig. 7 is improved.

The advantage of 1km-NHM is not only for the realistic PFS. Figure 11 shows the distributions of the top values of 24-hour-accumulated precipitation amounts (24h-Top) with a horizontal grid size of 20 km that is calculated from a 15-day experiment data. Many grids of the 24h-Top that are larger than 300 mm day^{-1} are found in the 5km-NHM experiment (Fig. 11a), while the peak value of the 24h-Top is about 200 mm day^{-1} in the 20km-GCM experiment (Fig. 11c). This suggests that 5km-NHM is superior to 20km-GCM for the simulation of extremely heavy precipitation events. Moreover, for the 24h-Top in the 1km-NHM experiment, a cluster of the 24h-Top that is larger than 400 mm day^{-1} is found with a zonal band over the central portion of the Kyushu District.

Figure 12 shows a time series of the distribution of surface precipitation and the low-level wind of a precipitation system that brings the large 24h-Top zone in the 1km-NHM experiment. In the precipitation phenomenon, 20km-GCM simulates a large precipitation cluster with a maximum precipitation intensity of about 10 mm h^{-1}. On the other hand, 5km-NHM simulates several meso-β-scale (defined as 20-200km by Orlanski, 1975 [29]) precipitation clusters with heavy precipitation intensities

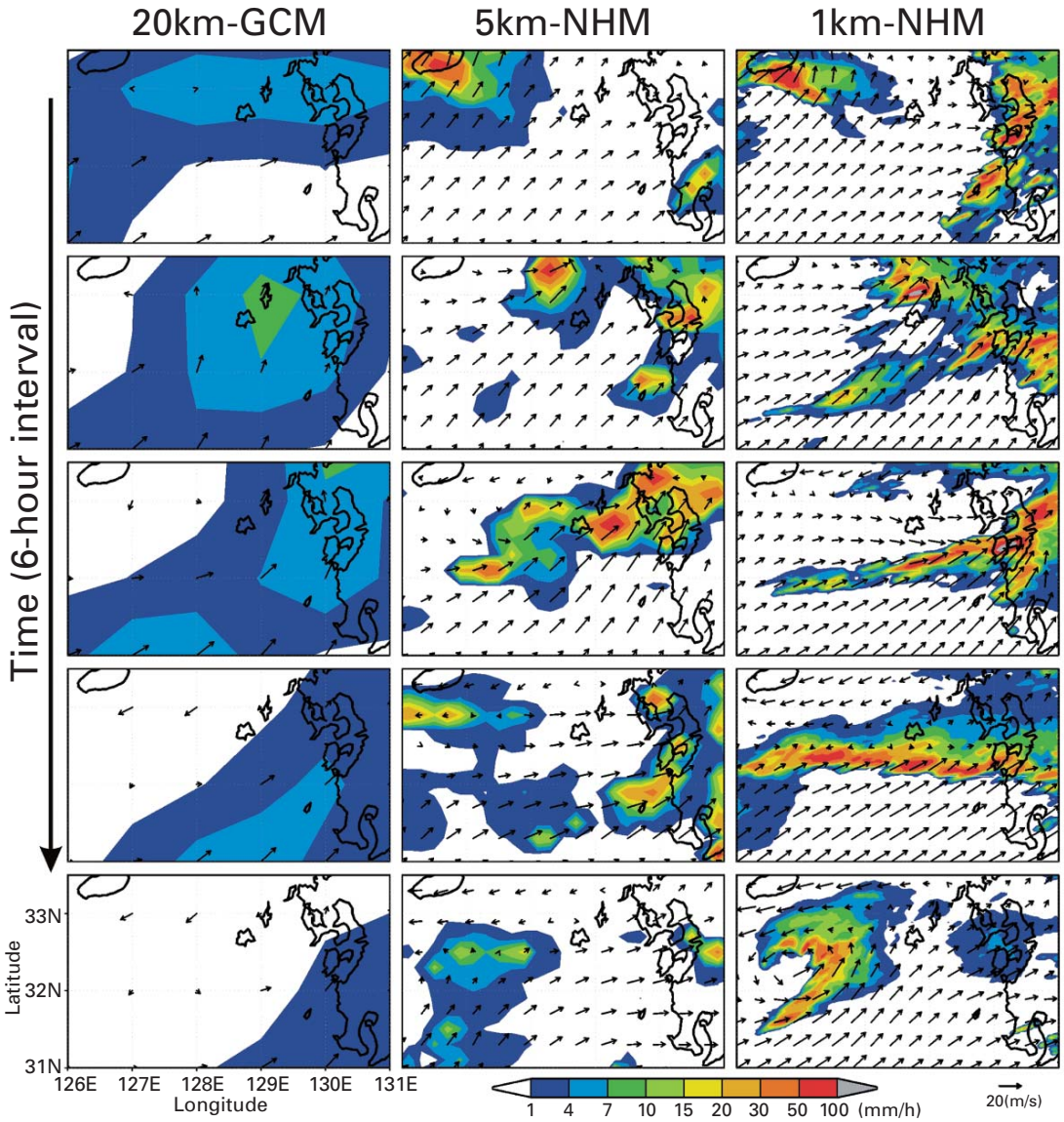

Fig. 12 Time series of the distributions of the surface hourly precipitation and horizontal wind at the 925 hPa level, focusing on the precipitation phenomenon, which produced the maximum value of 1km-NHM around the center of the Kyushu District (Fig. 11b) as an example. Left, center, and right panels are the results of 20km-GCM, 5km-NHM, and 1km-NHM, respectively.

above 50 mm h^{-1}. These precipitation clusters bring the large 24h-Top over the western part of the Kyushu District shown in Fig. 11a. Moreover, 1km-NHM simulates a zonal band-shaped precipitation system. The system contributes to the large 24h-Top with the zonal band shape. The band-shaped precipitation system is similar to that reported by Kato (1998) [30]. He showed that a band-shaped precipitation system was maintained by the back-building-type process defined by Bluestein and Jain (1985) [31]. A new cumulonimbus cloud is successively generated by the convergence of environmental low-level wind and divergence wind cased by an old cumulonimbus cloud. Consequently, such precipitation systems are organized by the interaction between the environment and cumulonimbus. The organized precipitation systems are often observed and sometimes cause extremely heavy precipitation events with serious disasters. Therefore, high-resolution experiments, such as that with 1km-NHM, might be required to reproduce extremely heavy rainfall events. Further statistical investigations with regard to the dependency on the grid size to represent the characteristics of extreme precipitation events will be needed. On the other hand, the high-resolution experiment generally requires a large cost for computational resources. Computers with more progressed performance than the ES will be needed for future statistical climatological calculations using 1km-NHM.

6. Summary

Regional climate experiments using NHMs of two different horizontal resolutions, 5km-NHM and 1km-NHM, were performed with a time-slice method to reproduce and project the Baiu frontal precipitation in the present and future climate, respectively. The boundary conditions of the 5km-NHM were taken from a time-slice experiment using a 20km-GCM. A downscale nesting experiment with 5km-NHM showed that the fine structures of the Baiu frontal precipitation are well reproduced, because the large-scale structures of the Baiu frontal precipitation are well reproduced by the 20km-GCM. The reproducibility of 5km-NHM in the present climate was examined. The 5km-NHM showed much better performances for the precipitation distribution and the PFS than the 20km-GCM.

In the future climate, the precipitation amounts increases mainly in Western Japan and decreases in Northern Japan. This is due to the elongation of the Baiu season and stagnation of the Baiu front associated with the changes in large-scale circulations. Another notable change is due to global warming, in which the precipitation is intensified in almost all regions around Japan. For example, the increased rate of precipitation is estimated to be about 1.9 for an intensity of 30 mm h^{-1} with a grid size of 20 km in the KS region.

The performance of the 1km-NHM was also examined. The experiments with the 1km-NHM were limited because of the large amount of computer resources required. However, it is suggested that the 1km-NHM can reproduce a more realistic PFS than 5km-NHM. In addition, it is also suggested that convective parameterization schemes are needed for the realistic PFS of the 5km-NHM experiments. Moreover, the 1km-NHM can accurately simulate extremely heavy precipitation events in comparison with the 5km-NHM and 20km-GCM. This suggests that a horizontal resolution of 1 km can express the organization of convective systems that cause extremely heavy precipitation.

Finally, this study suggests that the regional climate experiments using the NHM provide better performance for projecting regional climate changes, especially, for precipitation events. Here, the best performance depends on the reproducibility of the boundary data provided by the 20km-GCM within the defined regional domain for the NHM. Further improvements and developments of the NHM and AGCM in the future are expected for the projection of climate changes in precipitation with better quality.

Acknowledgements

This study was conducted under the framework of the Research Revolution 2002 (RR2002) project "Kyosei-4: Development of Super-High-Resolution Global and Regional Climate Models," funded by the Ministry of Education, Culture, Sports, Science, and Technology (MEXT). We thank Drs. T. Matsuo and T. Aoki and other members of the Kyosei-4 group who belong to the Japan Meteorological Agency (JMA) and the Meteorological Research Institute of JMA, and the Advanced Earth Science & Technology Organization (AESTO). The advice from Dr. K. Saito (MRI) was also very helpful. Thanks are extended to the reviewer of this paper.

(This article is reviewed by Dr. Julia Slingo.)

References

[1] IPCC (Intergovernmental Panel on Climate Change), 2001: *Climate Change 2001: The Scientific Basis*. Cambridge Univ. Press, 881pp.

[2] K. Ninomiya, and T. Akiyama, Multi-scale features of Baiu, the summer monsoon over Japan and the East Asia, *J. Meteor. Soc. Japan*, vol.**70**, pp.467–495, 1992.

[3] M. Kimoto, N. Yasutomi, C. Yokoyama, and S. Emori, Projected changes in precipitation characteristics around Japan under the global warming, *SOLA*, vol.**1**, pp.85–88, 2005.

[4] R. Mizuta, K. Oouchi, H. Yoshimura, A. Noda, K. Katayama, S. Yukimoto, M. Hosaka, S. Kusunoki, H. Kawai, and M. Nakagawa, 20-km-mesh global climate simulations using JMA-GSM model -Mean climate states-, *J. Meteor. Soc. Japan*, vol.**84**, pp.165–185, 2006.

[5] S. Kusunoki, J. Yoshimura, H. Yoshimura, A. Noda, K. Oouchi, and R. Mizuta, Change of Baiu rain band in global warming projection by an atmospheric general circulation model with a 20-km grid size, *J. Meteor. Soc. Japan*, vol.**84**, pp.581–611, 2006.

[6] J. Yoshimura, M. Sugi, and A. Noda, Influence of greenhouse warming on tropical cyclone frequency, *J. Meteor. Soc. Japan*, vol.**84**, pp.405–428, 2006.

[7] K. Oouchi, J. Yoshimura, H. Yoshimura, R. Mizuta, S. Kusunoki, and A. Noda, Tropical cyclone climatology in a global-warming climate as simulated in a 20 km-mesh global atmospheric model: frequency and wind intensity analyses, *J. Meteor. Soc. Japan*, vol.**84**, pp.259–276, 2006.

[8] Y. Wang, L. R. Leung, J. L. Mcgregor, D. Lee, W. Wang, Y. Ding, and F. Kimura, Regional Climate Modeling: Progress, Challenges, and Prospects, *J. Meteor. Soc. Japan*, vol.**82**, pp.1599–1628, 2004.

[9] K. Kurihara, K. Ishihara, H. Sasaki, Y. Fukuyama, H. Saitou, I. Takayabu, K. Murazaki, Y. Sato, S. Yukimoto, and A. Noda, Projection of climatic change over Japan due to global warming by high-resolution regional climate model in MRI, *SOLA*, vol.**1**, pp.97–100, 2005.

[10] H. Sasaki, K. Kurihara, and I. Takayabu, Comparison of climatic reproducibility between a super-high-resolution atmosphere general circulation model and a meteorological research institute regional climate model, *SOLA*, vol.**1**, pp.1–84, 2005.

[11] M. Yoshizaki, C. Muroi, S. Kanada, Y. Wakazuki, K. Yasunaga, A. Hashimoto, T. Kato, K. Kurihara, A. Noda, and S. Kusunoki, Changes of Baiu (Mei-yu) frontal activity in the global warming climate simulated by a non-hydrostatic regional model, *SOLA*, vol.**1**, pp.25–28, 2005.

[12] K. Yasunaga, H. Sasaki, Y. Wakazuki, T. Kato, C. Muroi, A. Hashimoto, S Kanada, K. Kurihara, M. Yoshizaki, and Y. Sato, Performance of the long-term integrations of the Japan Meteorological Agency nonhydrostatic model with use of the spectral boundary coupling method, *Weather and Forecasting*, vol.**20**, pp.1061–1072, 2005.

[13] K. Yasunaga, M. Yoshizaki, Y. Wakazuki, C. Muroi, K. Kurihara, A. Hashimoto, S. Kanada, T. Kato, S. Kusunoki, K. Oouchi, H. Yoshimura, R. Mizuta, and A. Noda, Changes in the Baiu frontal activity in the global warming climate simulated by super-high-resolution global and cloud-resolving regional climate models, *J. Meteor. Soc. Japan*, vol.**84**, pp.199–220, 2006.

[14] Y. Wakazuki, M. Yoshizaki, K. Yasunaga, C. Muroi, S. Kanada, A. Hashimoto, T. Kato, K. Kurihara, and A. Noda, Changes in the characteristic features of disturbances appearing in the Baiu frontal zone over Western Japan due to global warming, *SOLA*, vol.**1**, pp.129–132, 2005.

[15] S. Kanada, C. Muroi, Y. Wakazuki, K. Yasunaga, A. Hashimoto, T. Kato, K. Kurihara, M. Yoshizaki, and A. Noda, Structure of mesoscale convective systems during the late Baiu season in the global warming climate simulated by a non-hydrostatic regional model, *SOLA*, vol.**1**, pp.117–120, 2005.

[16] A. Hashimoto, M. Murakami, C. Muroi, M. Yoshizaki, Y. Wakazuki, S. Kanada, K. Yasunaga, T. Kato, K. Kurihara, and A. Noda, Characteristics of the averaged vertical profiles of hydrometeors in the Baiu season simulated with a non-hydrostatic regional climate model, *SOLA*, vol.**1**, pp.141–144, 2005.

[17] S. Yukimoto, A. Noda, A. Kitoh, M. Hosaka, H. Yoshimura, T. Uchiyama, K. Shibata, O. Arakawa, and S. Kusunoki, Present-day climate and climate sensitivity in the meteorological research institute coupled GCM version 2.3 (MRI-CGCM2.3), *J. Meteor. Soc. Japan*, vol.**84**, pp.333–363, 2006.

[18] K. Saito, T. Fujita, Y. Yamada, J. Ishida, Y. Kumagai, K. Aranami, S. Ohmori, R. Nagasawa, S. Kumagai, C. Muroi, T. Kato, H. Eito, and Y. Yamazaki, The operational JMA nonhydrostatic mesoscale model, *Mon. Wea. Rev.*, vol.**134**, pp.1266–1298, 2006.

[19] M. Ikawa, and K. Saito, Description of a nonhydrostatic model developed at the forecast research department of the MRI, *Technical Reports of the Meteorological Research Institute*, vol.**28**, 238pp, 1991.

[20] J. W. Deardorff, Stratocumulus-capped mixied layers derived from a three-dimensional mode, *Bound.-Layer Meteor.*, vol.**18**, pp.495–527, 1980.

[21] J. Kain, The Kain-Fritsch convective parameterization: An update, *J. Appl. Meteor.*, vol.**43**, 170–181, 2004.

[22] W. Y. Sun, and C. Z. Chang, Diffusion model for a convective layer. Part I: Numerical simulation of convective boundary layer, *J. Climate Appl. Meteor.*, vol.**25**, pp.1445–1453, 1986.

[23] J. F. Louis, M. Tiedtke, and J. F. Geleyn, A short history of the operational PBL parameterization at ECMWF, *Proc. Workshop on Planetary Boundary Parameterization*, Reading, United Kingdom, ECMWF, pp.59–79, 1982.

[24] J. Kondo, Air-sea bulk transfer coefficients in diabatic conditions, *Bound.-Layer Meteor.*, vol.**9**, pp.91–112, 1975.

[25] A. C. M. Beljaars, The parameterization of surface fluxes in large-scale models under free convection, *Q. J. R. Meteor. Soc.*, vol.**121**, pp.255–270, 1995.

[26] T. Tokioka, A stability study of medium-scale disturbances with inclusion of convective effects, *J. Meteor. Soc. Japan*, vol.**51**, pp.1–10, 1973.

[27] W. Yanase, and H. Niino, Structure and energetics of non-geostrophic non-hydrostatic baroclinic instability wave with and without convective heating, *J. Meteor. Soc. Japan*, vol.**82**, pp.1261–1279, 2004.

[28] H. Tagami, Meso-α-scale disturbances on the Baiu-front and their environmental field, *Doctoral dissertation*, 2005.

[29] I. Orlanski, A rational subdivision of scales for atmospheric processes, *Bull. Amer. Meteor. Soc*., vol.**56**, pp.527–530, 1975.

[30] T. Kato, Numerical simulation of the band-shaped torrential rain observed over southern Kyushu, Japan on 1 August 1993, *J. Meteor. Soc. Japan*, vol.**76**, pp.97–128, 1998.

[31] H. B. Bluestein, and M. H. Jain, Formation of mesoscale lines of precipitation - Severe squall lines in Oklahoma during the spring, *J. Atmos. Sci*., vol.**42**, pp.1711–1732, 1985.